Biosensors and Bioelectronics 66 (2015) 405–411

Contents lists available at ScienceDirect

Biosensors and Bioelectronics

journal homepage: www.elsevier.com/locate/bios

Turn-on optomagnetic bacterial DNA sequence detection using volume-amplified magnetic nanobeads

Rebecca S. Bejhed [a], Teresa Zardán Gómez de la Torre [a], Marco Donolato [b], Mikkel F. Hansen [b], Peter Svedlindh [a], Mattias Strömberg [a,*]

[a] Department of Engineering Sciences, Uppsala University, Box 534, SE-751 21 Uppsala, Sweden
[b] Department of Micro- and Nanotechnology, Technical University of Denmark, DTU Nanotech, Building 345 East, DK-2800 Kgs. Lyngby, Denmark

ARTICLE INFO

Article history:
Received 6 October 2014
Received in revised form
24 November 2014
Accepted 25 November 2014
Available online 29 November 2014

Keywords:
Optomagnetic system
Oligonucleotide-tagged magnetic beads
Padlock probes
Rolling circle amplification
Brownian relaxation
Phase angle spectra.

ABSTRACT

Detection of a *Vibrio cholerae* DNA-sequence using an optomagnetic read-out exploiting the dynamic behavior of magnetic nanobeads along with two *turn-on* data analysis approaches is demonstrated. The optomagnetic method uses a weak uniaxial AC magnetic field of varying frequency applied perpendicular to the optical path and measures the modulation of laser light passing through a cuvette containing the sample with oligonucleotide-tagged magnetic beads and macromolecular coils of single-stranded DNA. The DNA coils are formed upon a padlock probe ligation followed by rolling circle amplification (RCA). The presence of target gives rise to a change of the 2nd harmonic component, $V_2 = V_2' + iV_2''$, of the transmitted light. We demonstrate that by using the phase angle ξ defined as $\xi = \arctan(V_2''/V_2')$ in the low-frequency region we obtain a limit of detection of 10 pM for an RCA time of only 20 min corresponding to a total assay time of 60 min. Moreover, we show that the approach based on ξ is significantly more robust than the analysis based on a turn-off of the signal due to free magnetic nanobeads used in previous work (Donolato et al., submitted for publication), where a limit of detection of 10 pM was obtained for an RCA time of 60 min. The increased robustness and the reduction in total assay time constitute significant steps towards the realization of a low-cost, rapid and sensitive biosensor platform suitable for pathogen detection in both human and veterinary medicine settings.

1. Introduction

There is a growing interest in both industry and academia to develop simple, cost-efficient and rapid biosensor technologies. Applications range from fields such as human and animal health (Ivnitski et al., 1999; Lazcka et al., 2007; Luppa et al., 2011; Sanvicens et al., 2009; Schmitt and Henderson, 2005; Tothill, 2001; Wilson and Gifford, 2005), food safety (Amine et al., 2006; Arora et al., 2011; Ivnitski et al., 2000; Leonard et al., 2003; Mello and Kubota, 2002; O'Kennedy et al., 2005; Patel, 2002; Van Dorst et al., 2010; Velusamy et al., 2010), environmental monitoring, including biological threat agents detection (Amine et al., 2006; Iqbal et al., 2000; Rodriguez-Mozaz et al., 2004, 2005; Rogers, 1995; Rogers and Gerlach, 1999; Van Dorst et al., 2010; Velasco-Garcia and Mottram, 2003) to analysis of drinking water quality (Leonard et al., 2003; Mello and Kubota, 2002; Noble and Weisberg, 2005; O'Kennedy et al., 2005). Among the large number of existing biosensor types, e.g. electrochemical, (Grieshaber et al., 2008; Pumera et al., 2007) acoustic (Lange et al., 2008) and optical (Borisov and Wolfbeis, 2008; Fan et al., 2008), magnetic biosensors are particularly attractive due to a number of unique advantages (Koh and Josephson, 2009; Llandro et al., 2010). For instance, magnetic bead labels can be detected with very low background, their signal is stable over time and the associated read-out equipment can potentially be made at low cost. This means that magnetic biodetection devices have great potential to be used in resource-poor regions of the world (Yager et al., 2008). Also, magnetic beads could be used to enhance the performance of already existing biosensors and assays. One such example is the well-known latex agglutination test (LAT), which utilizes the formation of clusters of functionalized nanobeads as a read-out method (Ortega-Vinuesa and Bastos-Gonzalez, 2001; Singer and Plotz, 1956), the limit of detection (LOD) for the traditional LATs is approximately 1 nM (Baudry et al., 2006; Price and Newman, 1991).

Magnetic biosensors can be divided into two categories; surface-based and volume-based. Surface-based sensors utilize read-out elements consisting of sensor surfaces, such as magnetoresistive thin film elements, which can be functionalized with biomolecules (Janssen et al., 2008; Martins et al., 2009; Wang and

* Corresponding author.
E-mail address: mattias.stromberg@angstrom.uu.se (M. Strömberg).

http://dx.doi.org/10.1016/j.bios.2014.11.048

Li, 2008). This implies that they are only sensitive to magnetic particles in close vicinity to the sensor surface (Squires et al., 2008). Volume-based sensors, on the other hand, probe the entire sample volume. One example of a volume-based sensor is the optomagnetic sensor, where magnetic bead doublets formed through probe–target linkage are recognized optically, either through a change in optical transmittance or scattered light (Baudry et al., 2006; Park et al., 2009; Ranzoni et al., 2011). Another example of volume-based magnetic biosensing is Brownian relaxation bioassays relying on the change in frequency-dependent magnetic properties of magnetic nanobeads upon binding of a target analyte to the surface of probe-conjugated magnetic beads (Astalan et al., 2004; Connolly and Pierre, 2001). In the case of DNA detection, this change in Brownian relaxation dynamics can be strongly enhanced by letting detection probe conjugated beads attach to DNA coils produced by rolling circle amplification (RCA) of circularized DNA formed by padlock probe recognition of the target DNA (Strömberg et al., 2008). This particular bioassay method, denoted as the volume-amplified magnetic nanobead detection assay (VAM-NDA), makes use of isothermal amplification in combination with a homogeneous magnetic read-out, thereby yielding a high sensitivity and simplified sample preparation. It should be noted that the padlock probe ligation reaction constitutes highly specific target recognition since both the 5′ and 3′ ends of the linear padlock probe are designed to base-pair next to each other on the target strand. The VAM-NDA has been demonstrated for sensitive (low pM range) detection of bacterial DNA and spores as well as for studies of drug resistance in *Mycobacterium Tuberculosis* (Dalslet et al., 2011; Engström et al., 2013; de la Torre et al., 2012). However, these studies have used bulky and/or costly AC susceptometer equipments in most cases.

Recently, one major step towards a miniaturized and low-cost biodetection platform relying on the VAM-NDA was taken by demonstrating detection of DNA coils formed from a *Vibrio Cholerae* DNA target using a novel optomagnetic approach (Donolato et al., submitted for publication). In this approach the intensity of light transmitted through a magnetic nanobead dispersion is modulated by the application of a weak uniaxial AC magnetic field. In the presence of the magnetic field, the magnetic nanobeads align their magnetic moments preferentially along the field direction and might also form chain-like structures resulting in a modulation of the transmitted light at twice the frequency of the magnetic field. The ability of the magnetic nanobeads to follow the AC magnetic field depends on their hydrodynamic sizes. Thus, magnetic nanobeads that are free to rotate can follow the AC magnetic field to higher frequencies than nanobeads bound to DNA coils. By measuring the modulation of the transmitted laser light passing through the sample, or to be more precise the dependence of the 2nd harmonic component, $V_2 = V_2' + iV_2''$ of the transmitted light on the frequency of the AC magnetic field, the target analyte concentration can be obtained. It was shown that V_2' exhibits a peak at a frequency related to the Brownian relaxation frequency of free beads and that an increasing DNA coil concentration gives rise to a suppression of the peak amplitude, i.e., a turn-off effect. A wide range of DNA coil concentrations was considered (0–1000 pM) and it was shown that concentrations up to 100 pM could be detected and distinguished from each other by using the dose–response curve. Moreover, using 100 nm beads, a LOD of 10 pM was achieved. Further information on the underlying theory and interpretation can be found in Supplementary Section S1 and Donolato et al. (submitted for publication).

In this paper we present two novel methodologies to analyze V_2 data in a *turn-on* manner based on (i) the magnitude of V_2' in the low-frequency region and on (ii) the magnitude of the phase angle, $\xi = \arctan\left(V_2'/V_2''\right)$, in the low-frequency region. It should be noted that $\xi = 2\phi$, where ϕ is the phase lag of the magnetic response with respect to the magnetic field excitation; further information relating to the theoretical model describing the optomagnetic response can be found in Supplementary Section S1. We use two different bead sizes, 100 nm and 250 nm. Furthermore, we explore the impact on the detection sensitivity varying the bead concentration, the amplitude of the AC magnetic field (B_0) and the enzymatic amplification time (RCA time). Overall, we present a new and refined version of the optomagnetic read-out methodology allowing for more robust measurements and shorter assay times without sacrificing sensitivity.

2. Experimental section

Sequences of targets, padlock probes and detection oligonucleotides can be found in Supplementary material, Table S1.

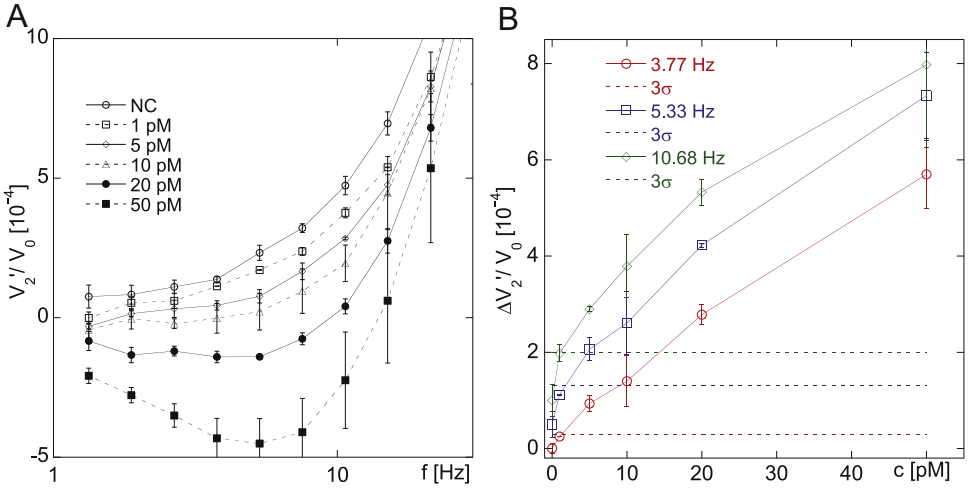

Fig. 1. Panel A displays representative low-frequency V_2'/V_0 spectra of samples containing 100 nm beads (100 μg/ml) and different DNA coil concentrations (NC to 50 pM), 60 min RCA time and $B_0 = 2.58$ mT. Panel B shows turn-on dose–response curves obtained by taking $\Delta V'_2/V_0 = V'_2(\mathrm{NC})/V_0(\mathrm{NC}) - V'_2(c)/V_0(c)$ at three different low-frequency points. The error bars correspond to one standard deviation (s.d.) obtained from triplicates. The dose–response curves in panel B are color coded and the dashed horizontal lines show the $\Delta V_2'/V_0$ mean value plus three s.d. (the LOD) obtained for the negative control sample at the indicated frequencies. Please note that for sake of clarity 0.5×10^{-4} and 1×10^{-4} have been added to the data to generate the blue and green curves in panel B, respectively. (For interpretation of the references to color in this figure legend, the reader is referred to the web version of this article.)

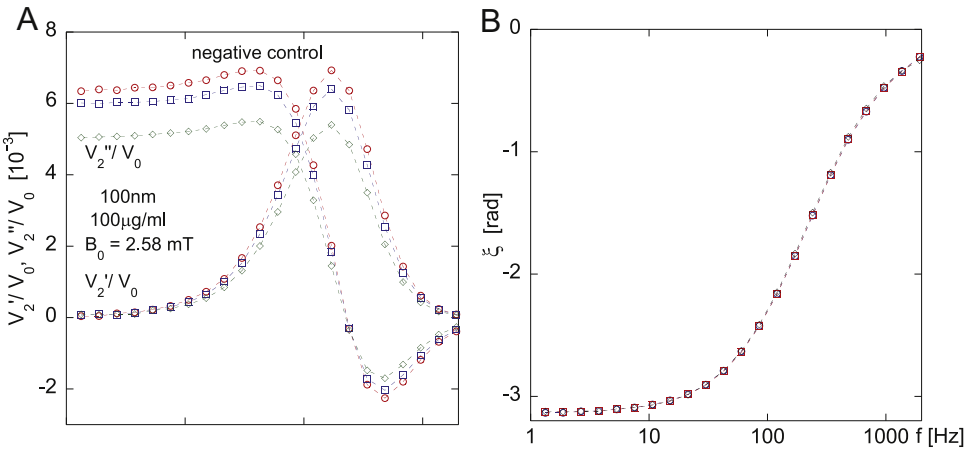

Fig. 2. Panel A shows V_2'/V_0 (lower set of curves) and V_2''/V_0 (upper set of curves) vs. frequency for three independent negative control samples containing 100 nm beads (100 μg/ml), B_0=2.58 mT. The curves in panel B show the phase angle $\xi = \arctan(V_2'/V_2')$ vs. frequency. The arctangent function is defined between $\pm\pi/2$. To obtain the phase curves as shown here, has been subtracted from all phase values below the frequency were the phase switches from $-\pi/2$ to $+\pi/2$. It should be noted that all three negative controls exhibit almost identical phase angle spectra as opposed to their V_2/V_0 representation.

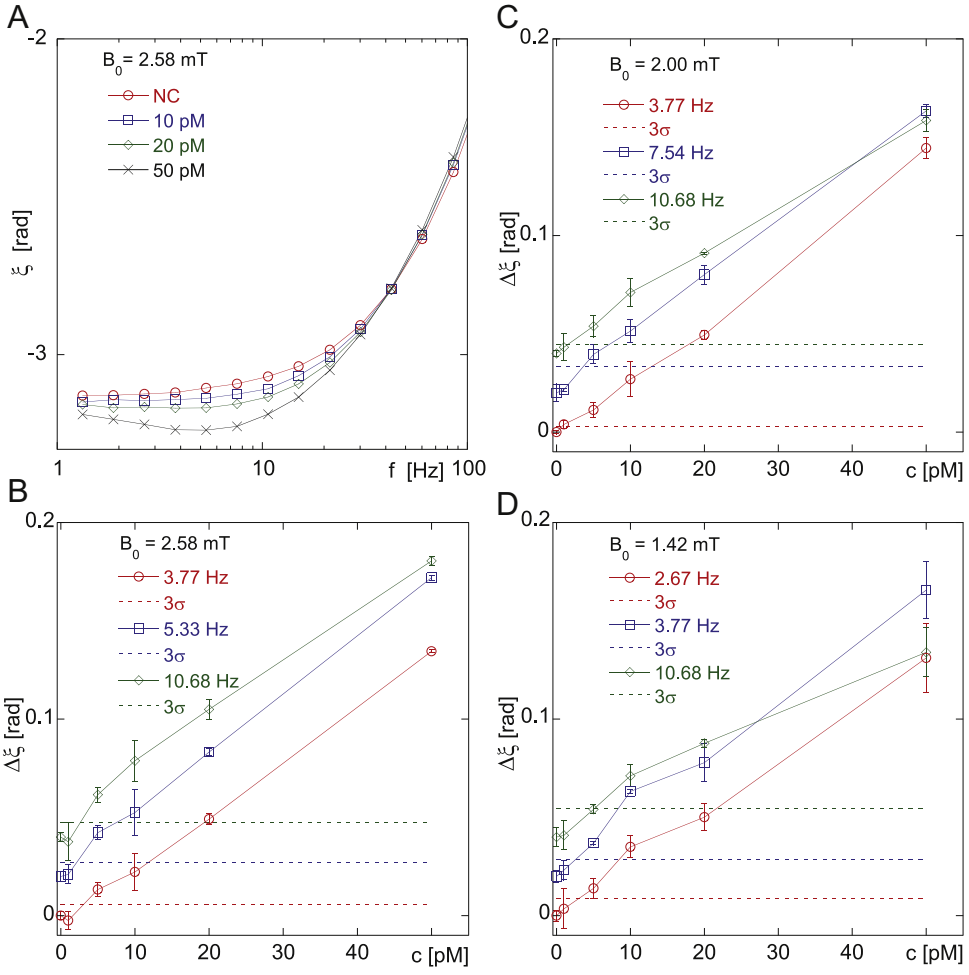

Fig. 3. Panel A displays ξ vs. frequency curves for samples with different concentrations of DNA coils (NC to 50 pM, 60 min RCA time) and 100 nm particles (100 μg/ml), B_0=2.58 mT. Panels B to D show $\Delta\xi = \xi(\mathrm{NC}) - \xi(c)$ vs. DNA coil concentration dose–response curves using different amplitudes of the AC field (2.58 mT to 1.42 mT in panels B to D). The dose–response curves are obtained by taking $\Delta\xi$ at three different low-frequency points. The error bars indicate one standard deviation (s.d.) based on triplicates. The dose–response curves in panels B to D are color coded and the dashed horizontal lines show the $\Delta\xi$ mean values plus three s.d. obtained for the negative control samples at the indicated frequencies. Please note that for sake of clarity 0.02 and 0.04 have been added to the data to generate the blue and green curves in panels B to D, respectively. (For interpretation of the references to color in this figure legend, the reader is referred to the web version of this article.)

2.1. Avidin–biotin conjugation of detection probes to magnetic nanobeads

Conjugations of biotinylated detection probes to 100 nm (BNF-Starch) and 250 nm (nanomag®-D) magnetic beads with avidin surface (Micromod, Germany) were performed according to protocols in Supplementary Section S2. The magnetic beads are of core shell type, where the core consists of a cluster of 5–15 nm sized maghemite crystals and the shell is made from either hydroxyethyl starch (100 nm beads) or dextran (250 nm beads). Conjugated bead suspensions of 2 mg/ml were further diluted with PBS to different concentrations (240, 320, 400 and 480 μg/ml of 100 nm beads; 200 μg/ml of 250 nm beads). Diluted bead suspensions were stored at 4 °C in sealed glass vials.

2.2. Padlock probe target recognition, ligation and rolling circle amplification

Solutions of 5 nM DNA coils (*V. cholerae* (*VC*) or *E. coli* (*EC*)) were synthesized according to protocols in Supplementary Section S3. Dilution series of DNA coils were prepared by stepwise dilution of the 5 nM DNA coil solution with hybridization buffer.

2.3. Optomagnetic measurement setup

The setup used for optomagnetic measurements is described in Supplementary Section S4. The output from one measurement is the total intensity, V_0, and the in-phase, V_2', and out-of-phase, V_2'', components of the complex second harmonic signal of the transmitted light. To compensate for variations in intensity of the laser light, amount of beads and reflection/absorption in the cuvette, all results of the second harmonic signal were normalized with the simultaneously measured values of V_0.

2.4. Optomagnetic measurements on samples containing DNA coils and oligonucleotide-tagged magnetic beads

Fifteen microliters of oligonucleotide-tagged bead solution (240, 320, 400 and 480 μg/ml of 100 nm beads; 200 μg/ml of 250 nm beads) was mixed with fifteen microliters of DNA coil solution of variable concentration *c* (4, 20, 40, 80 and 200 pM) or hybridization buffer in case of negative control (NC). The solution was incubated for 20 min at 55 °C and thereafter diluted with 30 μl of a 50–50 buffer mixture (50 v/v % of 1 × PBS pH 7.4 and 50 v/v% of hybridization buffer) followed by transferring the sample solution into a disposable cuvette (UV-Transparent Disposable, Order No. 67.758, optical path length 10 mm, Sarstedt, Germany). All

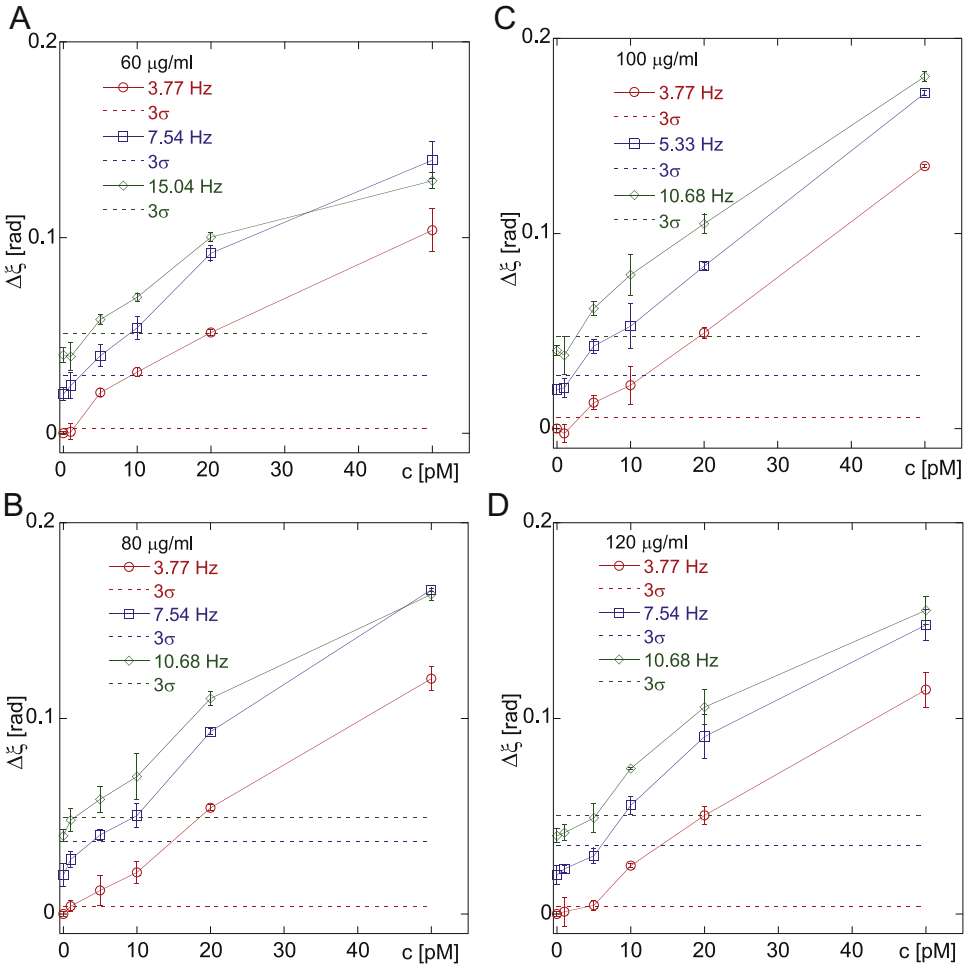

Fig. 4. $\Delta\xi$ vs. DNA coil concentration dose–response curves (B_0=2.58 mT, 60 min RCA time) obtained by taking $\Delta\xi$ at three different points in the low-frequency region for samples with different concentrations of 100 nm beads (60 μg/ml to 120 μg/ml in panels A to D). The error bars indicate one standard deviation (s.d.) based on triplicates. The dose–response curves are color coded and the dashed horizontal lines show the $\Delta\xi$ mean values plus three s.d. obtained for the negative control samples at the indicated frequencies. Please note that for sake of clarity 0.02 and 0.04 have been added to the data to generate the blue and green curves in panels A to D, respectively. (For interpretation of the references to color in this figure legend, the reader is referred to the web version of this article.)

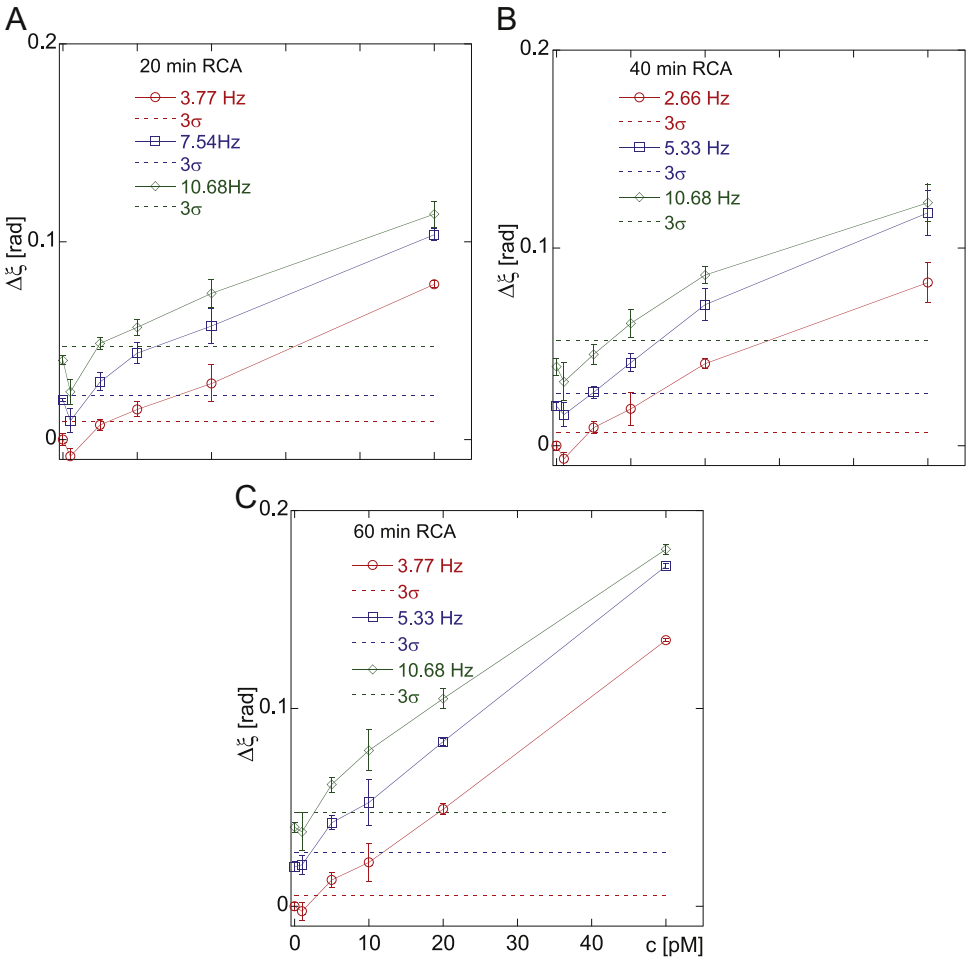

Fig. 5. Panels A to C display $\Delta\xi$ vs. DNA coil concentration dose–response curves for samples with 100 nm beads (100 μg/ml) and different RCA times ranging from 20 to 60 min (B_0=2.58 mT). The error bars indicate one standard deviation (s.d.) based on triplicates. The dose–response. curves are color coded and the dashed horizontal lines show the $\Delta\xi$ mean values plus three s.d. obtained for the negative control samples at the indicated frequencies. Please note that for sake of clarity 0.02 and 0.04 have been added to the data to generate the blue and green curves in panels A to C, respectively. (For interpretation of the references to color in this figure legend, the reader is referred to the web version of this article.)

DNA coil concentrations given below refer to the final concentration after mixing with the magnetic bead suspension and dilution with 50–50 buffer. Measurements of V_2 at room temperature were performed in the frequency range 1.33–2733 Hz (0.3–300 Hz) for 100 nm (250 nm) bead samples, using different AC magnetic field amplitudes (1.42, 2.00 and 2.58 mT).

3. Results and discussion

As mentioned in the introduction, the *turn-off* type read-out methodology applied in previous work (Donolato et al., submitted for publication) gave a limit of detection of around 10 pM for a bead size of 100 nm and an RCA time of 60 min. In the current work, the LOD is defined as the lowest tested amount of DNA yielding a normalized magnetic response differing with more than three standard deviations when compared to the negative control. It could be argued that it is generally, in biosensor contexts, more favorable with a response signal that increases with increasing analyte concentration. Thus, the next step would be to investigate different *turn-on* methodologies to analyze the normalized V_2 data. Furthermore, will such methodologies allow for a shorter assay time without sacrificing sensitivity? Also, it is highly relevant to search for more optimal assay conditions than that were was used in the previous study. With this in mind, we decided to first consider the normalized V_2' spectra in the low-frequency region, followed by examination of the phase angle spectra (obtained from the V_2' and V_2'' components). Moreover, one important objective of this study is to make a deeper investigation of how different experimental settings affect the performance of the assay, such as LOD, standard deviations and response difference between a NC and the highest analyte concentration. The parameters we chose to investigate were bead size, bead concentration, B_0 and RCA time.

Fig. 1A shows representative V_2'/V_0 spectra for samples with varying DNA coil concentrations (0–50 pM, 60 min RCA time, 100 μg/ml of 100 nm beads and B_0=2.58 mT). The effect of adding DNA coils is that the magnitude of the signal increases at low frequencies (turn-on). This signal change is attributed to magnetic nanobeads bound to DNA coils. In agreement with previous observations (Donolato et al., submitted for publication), where the optomagnetic signal as a function of magnetic bead size was studied, it is noted that the sign of this turn-on signal is opposite to that due to the free nanobeads. The turn-on effect is explained by the size-dependent scattering of objects, which depending on the ratio between the size of the object and the wavelength of light, may either increase or decrease the transmission when the AC magnetic field attains large values.

The corresponding dose–response curves obtained by taking $\Delta V_2'/V_0 = V_2'(\mathrm{NC})/V_0(\mathrm{NC}) - V_2'(c)/V_0(c)$ at three different low-frequency points are shown in panel B. With this turn-on methodology, the best LOD for 100 nm beads is 5 pM. However, it was

observed that the V_2/V_0 spectra within NC triplicates could differ considerably, especially around the V_2'/V_0 peak (see Fig. 2A), yielding large standard deviations. This motivated a search for an alternative turn-on approach making use of both V_2' and V_2'' data (see Fig. 2B) based on the phase angle of the V_2 signal, which has recently been used for analysis of magnetorelaxometry data (Dieckhoff et al., 2014; Schrittwieser et al., 2014). The rationale behind this method is that both components of V_2 will be similarly affected by changes in effective number of free magnetic nanobeads due to, e.g., beads adhering to the cuvette walls.

Panel A in Fig. 2 shows V_2'/V_0 (lower set of curves) and V_2''/V_0 (upper set of curves) vs. frequency obtained for three independent NC samples based on 100 nm beads with a bead content of 100 μg/ml ($B_0=2.58$ mT). The general behavior is in good agreement with the theory and interpretation described in Supplementary Section S1. As can be seen, the three V_2''/V_0 spectra deviate from each other mainly at low frequencies, whereas the V_2'/V_0 spectra deviate at higher frequencies. Panel B displays the phase angle, defined as $\xi = \arctan(V_2'/V_2'')$ vs. frequency for the V_2 spectra shown in panel A. The arctangent function is defined between $\pm\pi 2$. To obtain the phase curves as shown here, π has been subtracted from all phase values below the frequency where the phase switches from $-\pi/2$ to $+\pi/2$. As can be seen, the phase angle spectra for the three NC samples appear almost identical. We therefore consider the phase angle method as the most robust approach for a *turn-on* detection.

Fig. S3 shows V_2'/V_0 and V_2''/V_0 (panel A) and phase angle, ξ, spectra (panel C) vs. frequency for samples with 250 nm beads (50 μg/ml) and different concentrations of DNA coils (NC to 50 pM). It should be noted that the spectrum for the NC sample for the 250 nm beads shows the opposite sign compared to that of the 100 nm beads in agreement with previous observations (Donolato et al., submitted for publication). Upon increasing DNA coil concentration, the spectra show changes similar to those found for the 100 nm beads; the magnitude of the peak due to free magnetic nanobeads decreases and a signal of opposite sign (now positive) appears at low frequencies and is particularly clearly observed in the V_2''/V_0 data. Panels B and D display the dose–response curves $\Delta V_2'/V_0 = V_2'(c)/V_0(c) - V_2'(\mathrm{NC})/V_0(\mathrm{NC})$, taken at the high-frequency peak, and $\Delta\xi = \xi(\mathrm{NC}) - \xi(c)$, taken at three different frequencies in the low-frequency region, for the 250 nm beads. It can be concluded that an LOD of 20 pM can be reached with both *turn-off* and *turn-on* approaches; however, the sensitivity is not as high as when using 100 nm beads. Therefore, the optimization work was conducted solely using 100 nm beads. It may be argued that using even smaller beads (still exhibiting Brownian relaxation behavior) could give better detection sensitivity. Smaller beads would allow for V_2 measurements at higher frequencies, thus yielding more accurate measurements for the same measurement time. However, going below 100 nm bead size (while using the same type of multi-core beads of BNF-Starch type) makes the oligonucleotide conjugation protocol more complicated since the beads cannot be collected by standard permanent magnets.

Fig. 3A exemplifies the turn-on behavior of ξ for a bead size of 100 nm and different DNA coil concentrations when plotted as a function of frequency. Fig. 3B–D shows phase angle dose–respons curves vs. DNA coil concentration (60 min RCA time) for different amplitudes of the AC magnetic field (2.58 mT to 1.42 mT in panel B to D) using 100 nm beads (100 μg/ml). The corresponding phase angle spectra can be found in Supporting Fig. S4A–C. There seems to be a trend of slightly improved LOD and also increased response difference between the NC and 50 pM samples upon increasing field amplitude. We therefore consider it optimal to perform the read-out at large AC magnetic field amplitude.

Fig. 4 presents $\Delta\xi$ vs. DNA coil concentration dose–response curves ($B_0=2.58$ mT, 60 min RCA time) obtained by taking $\Delta\xi$ at three different frequencies in the low-frequency regime for samples with different concentrations of 100 nm beads (60 to 120 μg/ml in panel A to D). The corresponding phase angle vs. frequency spectra can be found in Supporting Fig. S5, A–D. The lowest LOD (5 pM) was found for 60, 80 and 100 μg/ml bead concentrations, but for 100 μg/ml bead concentration, the difference between the NC sample and the sample with the highest DNA coil concentration (50 pM) was found to be largest. Therefore, a bead concentration of 100 μg/ml was considered to be optimal. Going above 100 μg/ml gives a slightly higher LOD (10 pM). Moreover, it can be observed that for all considered bead concentrations, the obtained LOD is the same for all three frequency-points.

Fig. 5A–C display $\Delta\xi$ vs. DNA coil concentration dose–response curves.

($B_0=2.58$ mT) for samples with 100 nm beads (100 μg/ml) and for different RCA times. It can be observed that the LOD only slightly increases upon reducing the RCA time (5 pM for 60 min RCA and 10 pM for 40 and 20 min). In other words, with the phase angle approach, we reach the same sensitivity for 20 min RCA time as was obtained for 60 min RCA time in Donolato et al. (submitted for publication). The corresponding phase angle spectra and relative standard deviations of $\Delta\xi$ vs. DNA coil concentration can be found in Supporting Figs. S6 and S7, respectively. The main reasons for maintained sensitivity in the phase angle approach compared to previous studies (Donolato et al., submitted for publication) when using only 20 min RCA time are the higher measurement robustness (see Fig. 2) and the fact that the dose–response curves are derived from the low-frequency region where the response from beads bound to DNA coils is located.

Fig. S8 shows V_2'/V_0 (panel A), V_2''/V_0 (panel B) and phase angle (panel C) spectra for samples with 250 nm beads (50 μg/ml) and EC DNA coils (NC, 50 and 500 pM). The beads are functionalized with oligonucleotides complementary or non-complementary to the DNA coils. It can be seen that even a very high concentration of DNA coils non-complementary to the oligonucleotides on the beads does not give rise to a response change compared to the NC sample. Therefore, the change of V_2 upon varying the DNA coil concentration is solely due to the binding of beads to DNA coils.

The two turn-on readout principles presented above give rise to an increase in the low-frequency magnitude of V_2'/V_0 and ξ with increasing DNA coil concentration. According to Fig. 2A in Donolato et al. (submitted for publication, a small change in the total transmission when the AC magnetic field changes from zero to its maximum value (either positive or negative) can be observed (Donolato et al., submitted for publication). The sign of the change is related to whether the magnetic field aligned nanobead structures scatter the light more or less compared to the zero-field state as described in Supplementary Section S1. Moreover, the frequency range where the signal change appears depends inversely on the hydrodynamic volume of the relaxing entities and thus magnetic nanobeads bound to DNA coils give rise to a change in the signal at much lower frequencies compared to free magnetic nanobeads. This explains the increase of the magnitude of ξ in the low-frequency region upon increasing DNA coil concentration. In other words, at intermediate to low frequencies, beads bound in DNA coils are able to respond to the AC magnetic field, but with a phase lag. These coil bound beads give rise to the increase in the magnitude of V_2'/V_0, and a corresponding decrease in the magnitude of V_2''/V_0, at intermediate and low frequencies, with increasing DNA coil concentration. Both an increase in V_2'/V_0 and a decrease in V_2''/V_0 will increase ξ. At low enough frequencies, the increase in V_2'/V_0 turns into a decrease. It can be argued that this is an indication of that at low enough frequencies V_2'/V_0 will approach zero and the coil bound beads would also be in phase with the AC magnetic field. Thus, for low enough frequencies ξ will approach the value of π.

4. Summary and conclusion

We have successfully demonstrated two *turn-on* data analysis approaches for detection of *V. cholerae* DNA coils with a sensitivity of 5 pM. Optimal conditions were found through a systematic change of experimental parameters. The best LOD was reached by using 100 nm sized magnetic beads at a concentration of 100 μg/ml, AC magnetic field amplitude of 2.58 mT and 60 min of RCA time. The first analysis approach, based on the magnitude of V_2'/V_0 in the low-frequency region, exhibits a sensitivity of 5 pM, but the magnitude of the standard deviations is considered too large. Since variations between NC triplicates were observed in both the real and imaginary parts of the V_2/V_0 spectra, an assumption was made that some of these variations would be canceled out by an analysis approach taking both components of V_2 into consideration. Thus, the second analysis approach makes use of the phase angle of the V_2 spectra. Also with this approach, the ideal conditions were found to be 100 nm sized magnetic beads at a concentration of 100 μg/ml, AC magnetic field amplitude of 2.58 mT and 60 min of RCA time. Using the phase angle approach, the magnitude of the standard deviations was found to be significantly lower, although the LOD remained at 5 pM. Surprisingly, the sensitivity loss for detection of smaller DNA coils was almost negligible, opening up for the possibility to significantly shorten the whole assay time.

Overall, we have been able to demonstrate a new and refined version of the optomagnetic methodology, thereby taking steps further to the realization of a low-cost, rapid and sensitive biosensor platform suitable for pathogen detection in both human and veterinary medicine settings. Our next step will be to use this optimized system for detecting pathogenic bacteria using either the molecular protocols in the present work or an immunomagnetic approach. The current challenge in translating molecular diagnostics assays into a miniaturized format compatible with point-of care setting lies in the complexity of the sample preparation, DNA amplification process and the cost of the reader module, generally based on fluorescence. This work and the presented optomagnetic system tackle the challenge of simplifying the detection part, since it relies only on standard optical components and an electromagnet. The use of commercial magnetic nanobeads functionalized with complementary probes used in a homogeneous assay format circumvents the need for chip surface functionalization and washing. Moreover, the method has the distinct advantage of being compatible with any transparent microfluidic chip. Thanks to the presented advances, the LOD and dynamic range accessed in just 20 min amplification are comparable with current standard methods. Therefore the presented methodology holds a great potential to be integrated into an isothermal amplification-based molecular diagnostics device.

Acknowledgments

FORMAS (Project nos. 2011-1692 and 221–2012-444), The Swedish Foundation for Strategic Research and The Carl Trygger Foundation (Project no. CTS 12:554) are gratefully acknowledged for financial support. M.D acknowledges the support of the Ørsted post-doctoral grant.

Appendix A. Supplementary material

Supplementary data associated with this article can be found in the online version at http://dx.doi.org/10.1016/j.bios.2014.11.048.

References

Amine, A., Mohammadi, H., Bourais, I., Palleschi, G., 2006. Biosens. Bioelectron. 21 (8), 1405–1423.
Arora, P., Sindhu, A., Dilbaghi, N., Chaudhury, A., 2011. Biosens. Bioelectron. 28 (1), 1–12.
Astalan, A.P., Ahrentorp, F., Johansson, C., Larsson, K., Krozer, A., 2004. Biosens. Bioelectron. 19 (8), 945–951.
Baudry, J., Rouzeau, C., Goubault, C., Robic, C., Cohen-Tannoudji, L., Koenig, A., Bertrand, E., Bibette, J., 2006. Proc. Natl. Acad. Sci. USA 103 (44), 16076–16078.
Borisov, S.M., Wolfbeis, O.S., 2008. Chem. Rev. 108 (2), 423–461.
Connolly, J., St Pierre, T.G., 2001. J. Magn. Magn. Mater. 225 (1–2), 156–160.
de la Torre, Zardán G.ómez, Ke, T., Mezger, R., Svedlindh, A., Strømme, P., Nilsson, M., M., 2012. Small 8 (14), 2174–2177.
Dalslet, B.T., Damsgaard, C.D., Donolato, M., Strømme, M., Strömberg, M., Svedlindh, P., Hansen, M.F., 2011. Lab Chip 11 (2), 296–302.
Dieckhoff, J., Schilling, M., Ludwig, F., 2014. J. Appl. Phys. 115 (17).
Donolato, M., Antunes, P., Bejhed, R.S., Zardán Gómez de la Torre, T., Østerberg, F.W., Strömberg, M., Nilsson, M., Strømme, M., Svedlindh, P., Hansen, M.F., Vavassori, P., 2014. Anal. Chem. (submitted for publication).
Engström, A., Zardán Gómez de la Torre, T., Strömme, M., Nilsson, M., Herthnek, D., 2013. Plos One 8 (4), e62015.
Fan, X.D., White, I.M., Shopova, S.I., Zhu, H.Y., Suter, J.D., Sun, Y.Z., 2008. Anal. Chim. Acta 620 (1–2), 8–26.
Grieshaber, D., MacKenzie, R., Voros, J., Reimhult, E., 2008. Sensors-Basel 8 (3), 1400–1458.
Iqbal, S.S., Mayo, M.W., Bruno, J.G., Bronk, B.V., Batt, C.A., Chambers, J.P., 2000. Biosens. Bioelectron 15 (11–12), 549–578.
Ivnitski, D., Abdel-Hamid, I., Atanasov, P., Wilkins, E., 1999. Biosens. Bioelectron 14 (7), 599–624.
Ivnitski, D., Abdel-Hamid, I., Atanasov, P., Wilkins, E., Stricker, S., 2000. Electroanalysis 12 (5), 317–325.
Janssen, X.J.A., van IJzendoorn, L.J., Prins, M.W., 2008. Biosens. Bioelectron. 23 (6), 833–838.
Koh, I., Josephson, L., 2009. Sensors-Basel 9 (10), 8130–8145.
Lange, K., Rapp, B.E., Rapp, M., 2008. Anal. Bioanal. Chem. 391 (5), 1509–1519.
Lazcka, O., Del Campo, F.J., Munoz, F.X., 2007. Biosens. Bioelectron. 22 (7), 1205–1217.
Leonard, P., Hearty, S., Brennan, J., Dunne, L., Quinn, J., Chakraborty, T., O'Kennedy, R., 2003. Enzyme Microb. Tech. 32 (1), 3–13.
Llandro, J., Palfreyman, J.J., Ionescu, A., Barnes, C.H.W., 2010. Med. Biol. Eng. Comput. 48 (10), 977–998.
Luppa, P.B., Muller, C., Schlichtiger, A., Schlebusch, H., 2011. Trac-Trend Anal. Chem. 30 (6), 887–898.
Martins, V.C., Cardoso, F.A., Germano, J., Cardoso, S., Sousa, L., Piedade, M., Freitas, P. P., Fonseca, L.P., 2009. Biosens. Bioelectron. 24 (8), 2690–2695.
Mello, L.D., Kubota, L.T., 2002. Food Chem. 77 (2), 237–256.
Noble, R.T., Weisberg, S.B., 2005. J. Water Health 3 (4), 381–392.
O'Kennedy, R., Leonard, P., Hearty, S., Daly, S., Dillon, P., Brennan, J., Dunne, L., Darmaninsheehan, A., Stapleton, S., Tully, E., Quinn, J., Chakraborty, T., 2005. Rapid Methods: Biol. Chem. Contam. Food Feed, 85–104.
Ortega-Vinuesa, J.L., Bastos-Gonzalez, D., 2001. J. Biomater. Sci.-Polym. Ed. 12 (4), 379–408.
Park, S.Y., Handa, H., Sandhu, A., 2009. Nano Lett. 10 (2), 446–451.
Patel, P.D., 2002. Trac – Trend Anal. Chem. 21 (2), 96–115.
Price, C.P., Newman, D.J., 1997. Principles and Practice of Immunoassay. Macmillan Reference Limited.
Pumera, M., Sanchez, S., Ichinose, I., Tang, J., 2007. Sens. Actuat. B-Chem. 123 (2), 1195–1205.
Ranzoni, A., Schleipen, J.J.H.B., van Ijzendoorn, L.J., Prins, M.W.J., 2011. Nano Lett. 11 (5), 2017–2022.
Rodriguez-Mozaz, S., de Alda, M.J.L., Marco, M.P., Barcelo, D., 2005. Talanta 65 (2), 291–297.
Rodriguez-Mozaz, S., Marco, M.P., de Alda, M.J.L., Barcelo, D., 2004. Anal. Bioanal. Chem. 378 (3), 588–598.
Rogers, K.R., 1995. Biosens. Bioelectron. 10 (6–7), 533–541.
Rogers, K.R., Gerlach, C.L., 1999. Environ. Sci. Technol. 33 (23), 500A–506A.
Sanvicens, N., Pastells, C., Pascual, N., Marco, M.P., 2009. Trac – Trend Anal. Chem. 28 (11), 1243–1252.
Schmitt, B., Henderson, L., 2005. Rev. Sci. Tech. OIE 24 (1), 243–250.
Schrittwieser, S., Ludwig, F., Dieckhoff, J., Tschoepe, A., Guenther, A., Richter, M., Huetten, A., Brueckl, H., Schotter, J., 2014. Small 10 (2), 407–411.
Singer, J.M., Plotz, C.M., 1956. Am. J. Med. 21 (6), 888–892.
Squires, T.M., Messinger, R.J., Manalis, S.R., 2008. Nat. Biotechnol. 26 (4), 417–426.
Strömberg, M., Göransson, J., Gunnarsson, K., Nilsson, M., Svedlindh, P., Strømme, M., 2008. Nano Lett. 8 (3), 816–821.
Tothill, I.E., 2001. Comput. Electron. Agric. 30 (1–3), 205–218.
Van Dorst, B., Mehta, J., Bekaert, K., Rouah-Martin, E., De Coen, W., Dubruel, P., Blust, R., Robbens, J., 2010. Biosens. Bioelectron. 26 (4), 1178–1194.
Velasco-Garcia, M.N., Mottram, T., 2003. Biosyst. Eng. 84 (1), 1–12.
Velusamy, V., Arshak, K., Korostynska, O., Oliwa, K., Adley, C., 2010. Biotechnol. Adv. 28 (2), 232–254.
Wang, S.X., Li, G., 2008. IEEE Trans. Magn. 44 (7), 1687–1702.
Wilson, G.S., Gifford, R., 2005. Biosens. Bioelectron. 20 (12), 2388–2403.
Yager, P., Domingo, G.J., Gerdes, J., 2008. Annu. Rev. Biomed. Eng. 10, 107–144.